

DOCUMENT CONTROL SHEET

| | | | | | | | | | | | | | | | |
|---|--|-----------------------|--|-------------------|----------------------|-------------------|--------------|-------------|-----------------|-------------|---------------|-----------------|----------------|-------------|-------------------|
| | ORIGINATOR'S REF. TP 97409 U | | SECURITY CLASS. Unclassified | | | | | | | | | | | | |
| ORIGINATOR National Aerospace Laboratory NLR, Amsterdam, The Netherlands | | | | | | | | | | | | | | | |
| TITLE The Noise of a high-speed train pantograph as measured in the German-Dutch wind tunnel DNW | | | | | | | | | | | | | | | |
| PRESENTED AT: The 2 nd International Workshop on the AeroAcoustics of High-Speed Trains (AAT), Berlin, 29-30 April, 1997. | | | | | | | | | | | | | | | |
| PERMISSION The has granted NLR permission to publish this report. | | | | | | | | | | | | | | | |
| AUTHORS T. Dassen, P. Sijtsma, R. van Haaren, R. Parchen, K. Looijmans and H. Holthusen | | DATE 970821 | <table border="1" style="width: 100%; border-collapse: collapse;"> <tr> <td style="width: 50%;">pp</td> <td style="width: 50%;">ref</td> </tr> <tr> <td style="text-align: center;">21</td> <td style="text-align: center;">13</td> </tr> </table> | pp | ref | 21 | 13 | | | | | | | | |
| pp | ref | | | | | | | | | | | | | | |
| 21 | 13 | | | | | | | | | | | | | | |
| DESCRIPTORS <table style="width: 100%;"> <tr> <td style="width: 50%;">Acoustic emission</td> <td style="width: 50%;">Acoustic measurement</td> </tr> <tr> <td>Aerodynamic noise</td> <td>Aerodynamics</td> </tr> <tr> <td>Beamforming</td> <td>Data processing</td> </tr> <tr> <td>Measurement</td> <td>Noise (sound)</td> </tr> <tr> <td>Noise reduction</td> <td>Rail transport</td> </tr> <tr> <td>Windtunnels</td> <td>Wind tunnel tests</td> </tr> </table> | | | | Acoustic emission | Acoustic measurement | Aerodynamic noise | Aerodynamics | Beamforming | Data processing | Measurement | Noise (sound) | Noise reduction | Rail transport | Windtunnels | Wind tunnel tests |
| Acoustic emission | Acoustic measurement | | | | | | | | | | | | | | |
| Aerodynamic noise | Aerodynamics | | | | | | | | | | | | | | |
| Beamforming | Data processing | | | | | | | | | | | | | | |
| Measurement | Noise (sound) | | | | | | | | | | | | | | |
| Noise reduction | Rail transport | | | | | | | | | | | | | | |
| Windtunnels | Wind tunnel tests | | | | | | | | | | | | | | |
| ABSTRACT Two high-speed train tracks are planned to be realized in the Netherlands. These tracks will be supply links to France and Germany, at speeds up to 300 km/h. The connection Amsterdam-Paris should be realised in 2005, while travelling to Cologne at high speed will be possible in 2007. However, after the year 2000, the Netherlands law on railway noise becomes more than stringent: limits on railway noise levels (immission) will be reduced. Therefore different ways of reducing railway noise are investigated. At high train speed, above 200 km/h, rolling noise due to wheel/rail interacting no longer dominates the radiated noise. Aerodynamic sources become important at high-speed, since this noise is proportional to velocity with an exponent of about 6 to 7 (Ref. 1). For rolling noise the velocity exponent is about 3. Like for rolling noise, immission of aerodynamic noise can be reduced by taking measures at the source or by limiting the propagation of noise. Acoustic fencing by using noise barriers will require substantial parts of the high-speed tracks to be covered with barriers. Unlike rolling noise sources, aerodynamic sources are distributed over the total height of the train, with the pantograph representing a major source at 6 m above the track. Therefore it is expected that the noise radiated from the pantograph will determine the height of the barriers. | | | | | | | | | | | | | | | |

NLR TECHNICAL PUBLICATION

TP 97409 U

THE NOISE OF A HIGH-SPEED TRAIN PANTOGRAPH
AS MEASURED IN THE GERMAN-DUTCH WIND TUNNEL DNW

by

T. Dassen, P. Sijtsma, R. van Haaren^{*},
R. Parchen^{**}, K. Looijmans^{**} and H. Holthusen^{***}

This paper has been presented at the 2nd International Workshop on the AeroAcoustics of High-Speed Trains (AAT), Berlin, 29-30 April, 1997.

* NS Technisch Onderzoek NS-TNO

** TNO-TPD

*** German-Dutch Wind Tunnel

Division : Fluid Dynamics

Prepared : TD/~~PS~~ PS/ *PS*

Approved : HHB/ *HB*

Completed : 970821

Order number: 149.632

Typ. : MM



Contents

| | |
|--|----|
| Nomenclature | 5 |
| 1 Introduction | 5 |
| 2 Programme outline | 6 |
| 3 Experimental set-up and test programme | 6 |
| 3.1 The Adtranz DSA 350 SEK pantograph | 6 |
| 3.2 Experimental set-up | 6 |
| 3.3 Test configurations | 7 |
| 3.4 Test conditions | 7 |
| 4 The acoustic antenna | 7 |
| 4.1 Some backgrounds | 7 |
| 4.2 Data-processing | 7 |
| 5 Experimental results | 8 |
| 5.1 Acoustic images and noise spectra | 8 |
| 5.2 'Single' microphones spectra | 8 |
| 6 Model development and validation | 8 |
| 6.1 Modelling the aerodynamic noise of pantographs | 8 |
| 6.2 Analysis of DNW experiments on the aerodynamic noise of pantographs | 10 |
| 7 Conclusions | 11 |
| 8 Acknowledgement | 12 |
| References | 12 |
| 9 Figures | |

(21 pages in total)



This page is intentionally left blank.



The noise of a high-speed train pantograph as measured in the German-Dutch Wind Tunnel DNW

Ton Dassen, Pieter Sijtsma

National Aerospace Laboratory NLR, P.O. Box 153, NL-8300 AD Emmeloord
tel. +31.527.248642, fax. +31.527.248210, e-mail: dassen@nlr.nl

Rik van Haaren

NS Technisch Onderzoek NS-TO, Concordiastraat 67, NL-3551 EM Utrecht
tel. +31.30.2355160, fax. +31.30.2354163, e-mail: rikha@mail.nsto.ns.unisource.nl

Rene Parchen, Karel Looijmans

TNO Institute for Applied Physics TNO-TPD, P.O. Box 155, NL-2600 AD Delft
tel. +31.15.2692447, fax. +31.15.2692111, e-mail: parchen@tpd.tno.nl

Hermann Holthusen

German-Dutch Wind Tunnel DNW-LLF, P.O. Box 175, NL-8300 AD Emmeloord
tel. +31.527.248583, fax. +31.527.248582, e-mail: holthuse@nlr.nl

NOMENCLATURE

Roman

| | | |
|------------|--|------|
| c | chord length | m |
| c_0 | speed of sound | m/s |
| C_i | constants (see Eq. 9-12) | dB |
| d | typical length scale | m |
| Δf | frequency bandwidth | Hz |
| f | frequency | Hz |
| K | wave number | m |
| L | length | m |
| PWL | Sound Power Level (re. 1.10^{-12} Watt) | dB |
| r | distance to observer | m |
| s | span | m |
| SPL | Sound Pressure Level (re. 2.10^{-5} Pa) | dB |
| u | flow speed | m/s |
| U | tunnel flow speed | m/s |
| W | acoustic source strength | Watt |
| x | horizontal, streamwise co-ordinate | m |
| z | vertical co-ordinate | m |

Greek

| | | |
|-----------|-------------------------------|----------|
| δ | boundary-layer thickness | m |
| γ | turbulence correlation length | m |
| Λ | turbulence correlation length | m |
| ν | kinematic viscosity | m^2/s |
| ρ | ambient density | kg/m^3 |
| ϕ | spectrum function | - |
| ω | angular frequency | rad/s |

Indices

| | |
|-----|----------------------------------|
| 1/3 | 1/3-octave band |
| f | of frequency |
| hf | high-frequency |
| lf | low-frequency |
| max | maximum |
| p | of pressure |
| x | horizontal, streamwise component |
| ^ | non-dimensional |

Non-dimensional

| | |
|-----|------------------------------------|
| M | Mach number (u/c) |
| Re | Reynolds number ($u\delta/\nu$) |
| Str | Strouhal number ($f \times d/U$) |

1. Introduction

Two high-speed train tracks are planned to be realised in the Netherlands. These tracks will supply links to France and Germany, at speeds up to 300 km/h. The connection Amsterdam-Paris should be realised in 2005,

while travelling to Cologne at high-speed will be possible in 2007. However, after the year 2000, the Netherlands law on railway noise becomes more stringent: limits on railway noise levels (immission) will be reduced.

Therefore different ways of reducing railway noise are investigated. At high train speed, above 200 km/h, rolling noise due to wheel/rail interaction, no longer dominates the radiated noise. Aerodynamic

sources become more important at high-speed, since this noise is proportional to velocity with an exponent of about 6 to 7 (Ref. 1). For rolling noise the velocity exponent is about 3. Like for rolling noise, immission of aerodynamic noise can be reduced by taking measures at the source or by limiting the propagation of noise. Acoustic fencing by using noise barriers will require substantial parts of the high-speed track to be covered with barriers. Unlike rolling noise sources, aerodynamic sources are distributed over the total height of the train, with the pantograph representing a major source at 6 m above the track. Therefore it is expected that the noise radiated from the pantograph will determine the height of the barriers.

The area of pantograph noise prediction and reduction is rather 'unexplored'. Especially in the Netherlands, almost no research had been carried out till 1996. This is mainly due to the lack of Dutch pantograph and high-speed train manufacturers and due to the uncertain introduction of high-speed trains. In 1996 Technical Research of the Netherlands Railways initiated a research programme aimed at a better understanding of aeroacoustic noise sources at high-speed trains and the development and validation of prediction models. For this, the TNO Institute of Applied Physics TNO-TPD and the National Aerospace Laboratory NLR were contacted. These institutes already had experience on the modelling and reduction of flow-induced noise, from joint research on aerodynamic noise of wind turbines (Ref. [2,3]). Validated models for the aeroacoustic sources will supply useful tools for the prediction of the environmental impact of high-speed trains, but will also be very useful in designing low noise high-speed trains. Due to the importance of the pantograph noise, this component has been selected for the research described in this paper.

2. Programme outline

Mainly as a result of the limited amount of detailed information available in international literature, it was decided to 'explore' the radiation of aerodynamic noise from a pantograph, by performing a series of wind tunnel measurements on a full-scale pantograph. Wind tunnel testing is preferred as it allows for measuring a large number of configurations and conditions within a relatively short period of time.

As a testing facility, the German-Dutch Wind

Tunnel DNW was chosen. This tunnel, with its 8×6 m² open test section, allows for the full-scale testing of constructions like a pantograph.

In parallel, the development of prediction models using information presented in international literature, was taken in hand. After the measurements, results can then be used to validate these prediction models.

In this paper the results of the measurements and the development and validation of the models will be presented.

3. Experimental set-up and test programme

3.1 The Adtranz DSA 350 SEK pantograph

All measurements were performed on the DSA 350 SEK pantograph of Adtranz, made available to the project by the manufacturer Adtranz GmbH. Top and side views of this pantograph are presented in figure 1. In this figure, the most prominent parts and dimensions are indicated.

3.2 Experimental set-up

The pantograph measurements were performed in the open jet of DNW. In this configuration, an 8×6 m² exhaust nozzle is mounted approximately 19 m upstream of the 9.5×9.5 m² collector. The interjacent 19 m is called the open-jet test section. This section is surrounded by the DNW test hall which, in case of acoustic tests, is completely covered with sound absorbing material. The cut-off frequency (> 99% acoustic energy absorption) of this hall is approximately 200 Hz.

For practical reasons as well as to approach the real situation as much as possible, the pantograph was positioned on top of a 5×5.5 m² platform which was mounted to the lower lip of the exhaust nozzle.

An acoustic antenna (see next section) was placed aside, just outside the flow at approximately 1 m from the centre of the shear layer. The distance between the centre of the pantograph and the antenna was approximately 4.5 m. Two 'single' microphones were mounted to the ceiling of the test hall, 9.6 m above the top of the (extracted) pantograph.

Side, top and front views of the experimental set-up are given in figure 2a-c. The relevant dimensions are shown in these figures. The complete set-up is presented in figure a (sketch) and figure 3b (photographic picture also showing 'cones', see next section).

3.3 Test configurations

The measurements were started with the cylindrical parts of the head components wrapped in wires to eliminate the coherent shedding of vortices. With these wires present, measurements were done in the 'knee-backward position', with the pantograph down (parked) and up (head at 1.95 m). With the head up, measurements were performed on the complete pantograph and after the first (most upstream) contact strip or the last (downstream) contact strip, or both contact strips had been removed. In the last test both contact strips and the horns had been removed.

After all components had been mounted again measurements were also performed with disturbed flow. The disturbances were obtained by mounting 0.6 m high cones at the lower nozzle lip, 4 m upstream of the pantograph. The velocity and turbulence profiles and spectra downstream of these cones were known from previous measurements. The cones are shown in the photographic picture of figure 3b.

Measurements with the knee in backward position were also performed after the wires had been removed. During part of these measurements a load cell was mounted between head and base frame to measure the aerodynamic forces exerted on the pantograph head. Without wires and without load cell, measurements were only performed with the head of the pantograph at a somewhat lower position (1.60 m).

In the 'knee-forward position' no geometrical adjustments were made (complete pantograph with wires only) and measurements were performed only with clean (undisturbed) flow. In this configuration the pantograph was also rotated at an angle of 10° with respect to the flow direction.

Finally, measurements were performed after the complete pantograph had been removed, to measure the noise of the empty platform.

3.4 Test conditions

All configurations were tested at wind speeds of approximately 41, 54, 71, and 78 m/s (148, 194, 256 and 281 km/h or $M=0.12, 0.16, 0.21, \text{ and } 0.23$). With the wires removed (and the head at 1.6 m) measurements were additionally done at approximately 31, 48, and 65 m/s ($M=0.09, 0.14, \text{ and } 0.19$).

4. The acoustic antenna

4.1 Some backgrounds

In principle, acoustic focusing (also called 'beamforming') is based on 'comparing' the phases and amplitudes of the signals of a 'large' (typically some tens) number of microphones. Here, the positioning of the microphones with respect to each other and with respect to the model is of crucial importance. The gain (difference between peak level and highest side-lobe level), resolution and frequency range at which the antenna can be operated, depends on this positioning. It has to be noted that the gain can be improved, to a certain extent, after the measurements, by 'weighting' of the signals. This 'weighting' affects the level of side-lobes which appear as virtual sources in the acoustic image. The application of 'weighting' will reduce the side-lobe level, thus yielding an improvement of the gain, but will always lead to a worsening of the resolution.

The antenna used is a so-called nested configuration; a high concentration of microphones near the centre and a lower away from it. The positioning of the microphones further seems to be rather unstructured. This way of positioning offers the possibility to obtain a high resolution for a large range of frequencies. The reader interested in more details is referred to one of the textbooks about this topic (f.i. Ref. [4,5]).

The resolution resulting, expressed in -3 dB peak width, is less than 0.2 m (no 'weighting'), meaning that two equally strong sources can be distinguished if they are spaced by at least 0.3 m. Sources with strengths differing 3 or 6 dB can be distinguished only if they are spaced by at least 0.4 m and 0.6 m respectively. These values are valid for a frequency of 4 kHz. At 1 kHz and 2 kHz these values have to be multiplied by 4 and 2, respectively.

The gain, defined here as the difference between the level of the main lobe and the nearest side-lobe is approximately 8 dB (no 'weighting').

4.2 Data-processing

The antenna data-processing basically consists of the following steps:

1. The calculation of all autopower spectra and all mutual crosspower spectra.
2. A 'principal component analysis'. This analysis is used to filter out part of the noise (Ref. [6,7]).
3. The application of 'weighting' to suppress side-lobes (optional).

4. The scanning of a source plane using an 'adaptive beamforming' technique.

'Adaptive beamforming' offers a higher noise suppression than the conventional 'sum-and-delay beamforming' (Ref. [8,9]). The result of the scanning of a source plane is further indicated with 'acoustic image'. High levels in the acoustic image (peaks) may indicate the presence of a sound source. The highest value of the acoustic image at the source position can be used as a measure for the acoustic power radiated by that source. In the computations, a correction for the convection of the sound by the wind tunnel flow is included.

5. The calculation of Sound Power Levels under the assumption that the sound sources are monopoles.

6. The determination of narrowband spectra of the dominant noise sources from the level of the local maxima in the acoustic images. In the case of the pantograph, the spectra of the noise radiated from the region of the head, the knee and the base parts are determined using the acoustic images which can be obtained for all frequencies in the range of 520 Hz up to 6 kHz ($\Delta f=40$ Hz). Here, it has to be noted that maxima appearing in the regions around these parts can not always be reliably ascribed to the presence of a noise source. The procedure used to determine whether these maxima can be used to determine the Sound Power Level will not be explained in this paper.

5. Experimental results

5.1 Acoustic images and noise spectra

In figure 4a and 4b, typical acoustic images resulting from the scanning of a 2.5×3 m² plane around the centre of the pantograph, are given. In the images the position of the pantograph is indicated. Every individual image represents the integrated result of the scanning of all frequencies within one octave band.

Furthermore, the spectra of the noise radiated from the head, knee and base part were obtained. Some of these spectra are shown and compared to predictions (see section 6) in the figures 5 through 9. In many cases, spectra could not be determined completely for every part, due to the fact that the procedure, referred to in the previous paragraph, indicated that the spectral value could not be determined reliably.

Based on former experiences, acoustic images and/or spectra can be used reliably for comparing different configurations and conditions. Repeat

measurements have shown that the spreading in these results is less than 1 dB. However, the use of individual results in an absolute sense, is much more complicated. The reasons for this are various:

- The assumption of a distribution of monopole sources in the beamforming algorithm.

- The influence of the tunnel (shear-layer diffraction, reflections which occur at the platform and/or the antenna support). The regular pattern appearing at frequencies above 3 kHz in almost all spectra is expected to result from reflections.

- The frequency-dependent resolution and 'gain' of an antenna. From a previous experience using a well-known source for antenna calibration, it is estimated that this frequency dependency introduces uncertainties up to ± 2 dB at $M=0.12$ and ± 4 dB at $M=0.23$.

As a major consequence, it may be expected that the level will deviate from the correct values as well as that the shape of the spectra will be distorted. From former experiences it is known that the level of the spectra may be in error by up to ± 4 dB over the whole range of frequencies (750 Hz up to 6 kHz). As a rough estimate it is expected that the shape distortion may also be ± 4 dB maximally.

5.2 'Single' microphones spectra

After completion of the test it was found that several tonal peaks appear in the low-frequency part (100-500 Hz) of the spectra in case some components are not wrapped in wires. As the antenna was not designed for this frequency range, the signals of some 'single' microphones were processed as well.

The spectra of these microphones were corrected to compensate for the difference in distance to the model. Shear-layer and damping corrections, known to be limited to 1 dB typically, were not applied.

6. Model development and validation

6.1 Modelling the aerodynamic noise of pantographs

Aerodynamic noise of high-speed trains is produced by several parts which produce noise by different mechanisms. Examples of aerodynamic noise production by parts of the train are: broadband noise and tonal noise due to flow over cavities in the train wall (e.g., the gap between two coaches), broadband noise due to flow across protruding streamlined bodies (inflow-turbulence noise,

trailing-edge noise), and broadband noise and tonal noise due to vortex shedding at protruding streamlined and bluff bodies. In all cases interaction of vorticity in the flow with train parts are the basic mechanisms of noise production.

The pantograph is expected to be an important source of aerodynamic noise. It consists of a large number of streamlined and bluff bodies of different size and shape that protrude about 2 m above the train roof into the flow.

Noise generating mechanisms that are expected to be of importance for aerodynamic pantograph noise are listed in the next paragraphs.

Inflow-turbulence noise

Turbulence in the flow imposes a time-varying lift force on streamlined bodies. As a result, these bodies radiate broadband noise. Amiet (Ref.10) formulates a model that predicts noise production of non-compact objects due to inflow turbulence on the basis of an aerodynamic response function:

$$\text{SPL}_{1/3}^{\text{hf}} = 10 \log_{10} \left(\frac{sc}{r^2} M^5 \frac{\overline{u^2}}{U^2} \frac{\hat{K}_x^3}{(1 + \hat{K}_x^2)^{7/3}} \right) + 181.3, \quad (1)$$

where s is the span of the object, c is the chord length, and r the distance to the observer. The factor

$$\frac{\overline{u^2}}{U^2} \frac{\hat{K}_x^3}{(1 + \hat{K}_x^2)^{7/3}} \quad (2)$$

represents the power spectrum of velocity fluctuations, with K the wave number. In most cases relevant for train noise, the chord of the object can not be considered large compared to the wavelength of the noise. Therefore, for low frequencies the model of Amiet must be adapted. For compact bodies Amiet (Ref. 10) suggests a correction factor based upon the Sears function

$$\text{SPL}_{1/3}^{\text{lf}} = \text{SPL}_{1/3}^{\text{hf}} + 10 \log_{10} \left(M \frac{\pi^2 \hat{\omega}^2}{1 + 2\pi\hat{\omega}} \right), \quad (3)$$

in which $\hat{\omega}$ is a non-dimensional angular frequency: $\hat{\omega} = \pi f c / U$.

Applying this correction in the low frequency limit yields the classical M^6 dependence for the radiated sound power of a dipole source.

Turbulent boundary layer trailing-edge noise

Another source of aerodynamic broadband noise is the turbulent boundary layer trailing-edge noise. Pressure fluctuations caused by turbulence in the boundary layer of objects with sharp edges are scattered at the sharp edges as noise. An expression for the source strength of boundary layer trailing-edge noise can be formulated on the basis of an analysis by Dowling and Ffowcs Williams (Ref. 11) of the sound power produced by a single turbulent eddy passing a trailing edge. The analysis yields for boundary layer trailing-edge noise:

$$W \propto \frac{4\rho U^5 \frac{\overline{u^2}}{U^2} \delta^2}{\pi c_0^2} \quad (4)$$

Brooks, Pope and Marcolini (Ref. 12) combined the expression of the source strength with empirical data to formulate a prediction model for boundary layer trailing-edge noise of wind turbine blades. They propose a universal spectrum shape which depends on the Strouhal number:

$$\frac{(\text{Str}/\text{Str}_{\text{max}})^{5/2}}{((\text{Str}/\text{Str}_{\text{max}})^{5/2} + 1)^2}, \quad (5)$$

where Str_{max} represents the Strouhal number at which the noise spectrum exhibits its maximum. This Strouhal number is related to the boundary layer thickness according to:

$$\text{Str}_{\text{max}} \propto \text{Re}_\delta^{-0.6}. \quad (6)$$

Vortex-shedding noise

At most parts of the pantograph flow separation will occur. The vorticity shed in the wake of an object imposes a fluctuating force on the object that generates sound. Depending on the Reynolds number of the flow the wake is more or less turbulent. Below a critical Reynolds number which depends on the shape of the object, the vortex shedding is coherent and tonal noise can occur.

For larger Reynolds numbers the turbulence in the wake will generate broadband noise. Blake (Ref. 13) gives an expression for the broadband sound pressure level caused by turbulence in the wake of a cylinder:

$$\text{SPL} = 10 \log_{10} \left(\frac{L\Lambda - \gamma\Lambda}{r^2} M^6 \phi_{pp} \right) + C \quad (7)$$

with ϕ_{pp} a non-dimensional spectrum function

$$\phi_{pp} = \frac{\omega^2 d^2}{U_\infty^2} \phi_{ff}(\omega) \Delta\omega = \text{Str}_\omega^2 \hat{\phi}_{ff}(\text{Str}_\omega) \Delta\text{Str}_\omega, \quad (8)$$

where ϕ_{ff} represents a scaled force spectrum. L is the length of the object, and Λ and γ are two correlation lengths with respect to the turbulence in the wake. The shape of the spectrum function ϕ_{ff} depends on the Reynolds number.

For a Reynolds number smaller than 400, the spectrum function is sharply peaked around its maximum near a Strouhal number of 0.2. For larger Reynolds number the spectrum function broadens.

6.2 Analysis of DNW experiments on the aerodynamic noise of pantographs

The acoustic images of the pantograph (e.g., see figure 4) have shown that the strongest noise sources of the high speed train pantograph in the DNW are located in the top and base (foot) region. The knee region contributes significantly less to the noise radiation. This has been observed for the whole series of test configurations and conditions. Therefore, the following analysis will concentrate on noise production by the top and foot region of the pantograph.

Top region

Figure 5 shows the sound power level of the noise sources in the top region of the pantograph in the

standard geometry as a function of the Strouhal number based on the tunnel speed and on a typical length scale of

0.005 m which corresponds to the diameter of the lift limiters. In this configuration the lift limiters and other parts of the pantograph were not equipped with tire wraps. At a Strouhal number of 0.19 a peak is observed for the whole Mach number range from 0.09 up to 0.23. This indicates that coherent vortex shedding at the lift limiters occurs which produces a strong tonal sound. The noise spectrum exhibits a second tone at a Strouhal number of 0.05. This Strouhal number corresponds to vortex-shedding noise at a cylinder of 0.02 m which corresponds to the thickness of the horns. Hence, in the standard geometry the horns and lift limiters produce tonal noise.

To identify the parts of the pantograph that are the strongest noise sources, a series of antenna experiments were done with several parts of the pantograph removed. The horn and the lift limiters were equipped with tire wraps in these measurements. The results of the experiments at a tunnel Mach number of 0.23 are given in the 1/3rd octave plot of figure 6.

The sound power levels of the measurements on a complete pantograph, and on configurations in which the contact strips and the horns were removed, coincide within 1 dB over the whole frequency range. This shows that neither the contact strips nor the horns contribute significantly to the wayside radiated broadband noise. Therefore, it is expected that other parts such as the lift limiters are the largest sources of broadband noise in the top region. Reduction of noise radiation by the top of the pantograph can be achieved by optimisation of the pantograph top region.

In figure 7 the noise production of the top region is compared to the prediction of inflow-turbulence noise according to Amiet (eq. 3) and trailing-edge noise according to the method described by Brooks, Pope and Marcolini (Ref. 12) for a 1 m² flat plate. A turbulence intensity of 0.001 is an upper bound for the turbulence intensity in the top region during the experiment. A value of 0.05 is a representative value for a high-speed train.

The noise measurements on the pantograph exceed the prediction of inflow-turbulence noise for a turbulence intensity of 0.05 by about 10 dB. Therefore, it is expected that vortex-shedding noise is an important noise source. The result further suggests that by optimising the shape of the pantograph top region a reduction in the order of 10 dB can be obtained.



Foot (base part) region

The pantograph foot (base part) region is in the boundary layer of the train. In the boundary layer the inflow velocity is smaller than the velocity in the pantograph top region, but the turbulence intensity in the boundary layer will be much higher than in the top region. Consequently, the foot region is an important source of aerodynamic noise too. To study the effect of an increased turbulence level on sound production of the foot region an obstruction was placed in the inflow of the pantograph, consisting of an array of 'cones'. As a result of the installation of the cones the inflow velocity in the foot region reduces to 0.81 times the tunnel speed, at a height of 25 cm above the platform. The turbulence intensity increases by a factor 70 to 80.

In figure 8 a measurement at a tunnel Mach number of 0.16 without obstruction in the flow is compared to a measurement at a tunnel Mach number of 0.21 with obstruction. Due to the presence of the obstruction the flow velocities in the foot region are of comparable magnitude. The turbulence intensity will be a factor 90 larger for the flow with obstruction. The figure shows that the increase of turbulence intensity enhances the sound power level of the foot region by about 9 dB.

According to Amiet the sound power increases proportional to the square of the turbulence intensity, predicting an increase in sound power level by 39 dB. So, the measured increase of sound power level appears to be considerably smaller than the predicted increase, i.e. the noise radiation appears not to be proportional to the energy content of the turbulence. This suggests that inflow-turbulence noise is not the only source mechanism. If the turbulence level is decreased sufficiently, vortex-shedding noise probably becomes a significant source of noise in the foot region too.

Scaling and spectrum shape

By applying an appropriate scaling, all measurements at different tunnel speeds will collapse into one single curve, as is shown in figure 9. In this figure a scaled sound pressure level is given versus the Strouhal number based on a length of 0.05 m and on the tunnel speed. The Strouhal number bandwidth, ΔStr , is $5 \cdot 10^{-3}$. The scaled sound pressure level is based on the expression of broadband vortex-shedding noise (eq. 7), and is defined as:

The constant C_1 depends on a typical length scale L of the pantograph, the turbulence correlation length scales Λ and γ , and the distance to the

$$\begin{aligned} \text{ScaledSPL} &= \\ \text{SPL} - 10\log_{10}M^6 - C_1. \end{aligned} \quad (9)$$

observer r :

$$C_1 = 10\log_{10} \frac{L\Lambda - \gamma\Lambda}{r^2}. \quad (10)$$

In the present analysis C_1 was determined from the measurements.

On the basis of this scaling, a model can be formulated to predict the broadband aerodynamic noise of a pantograph. To describe the shape of the scaled sound pressure spectrum, a Strouhal number dependent shape factor *shape(Str)* is introduced. An expression for the Scaled SPL is then given by

$$\text{ScaledSPL} = \text{shape}(\text{Str}) + C_2, \quad (11)$$

where C_2 is a constant that was determined empirically.

So, the following correlation for the narrowband sound pressure level of the broadband noise is obtained:

$$\begin{aligned} \text{SPL} &= 10\log_{10}M^6 + \\ &\text{shape}(\text{Str}) + C_1 + C_2, \end{aligned} \quad (12)$$

where C_1 is defined by eq. (10). In figure 9, eq. (12) is given by the dashed curve. For low Strouhal numbers, the Scaled SPL and the correlation as expressed in eq. (12), deviate. As can be seen from the dashed and dotted curves, which represent the correlation and the measured noise level in an empty tunnel respectively, the lower part of the spectrum below a Strouhal number of 0.1 is dominated by background noise.

7. Conclusions

Measurements of the aerodynamic noise of an Adtranz DSA 350 SEK high-speed train pantograph were performed in the German Dutch Wind Tunnel DNW-LLF. Thirteen configurations, each at minimally four different wind speeds were tested, using an acoustic antenna and 'single' microphones.

The 'non-redundant' positioning of the antenna microphones in a plane of approximately $4 \times 4 \text{m}^2$, has proved to yield the gain and resolution expected



from simulations, i.e. the pantograph noise sources could be located and their relative contributions were determined.

For all configurations and conditions it is found that the top region and the foot region of the pantograph are the most dominant sources of aerodynamic noise. Comparison of different configurations give strong indications for the lift limiters being the most important source of broadband noise. Neither the contact strips, nor the horns were found to contribute significantly to the (wayside) total noise. It is also found that the standard (untreated) lift limiters and the horns are sources of tonal noise. The measurements further showed that increasing the level of inflow turbulence increases the sound power emitted by the foot region and that the measured sound pressure levels scale with M^6 .

The results of both the antenna and the 'single' microphones were analyzed and compared to predictions. For this, models were considered which describe the noise production resulting from i) vortex shedding from streamlined and bluff bodies, ii) interaction of boundary-layer turbulence with sharp edges, and iii) interaction of turbulence in the inflow with parts of the pantograph. These mechanisms generate broadband noise only, except for vortex shedding which can also be a source of tonal noise, depending on the Reynolds number of the flow. Depending on the 'compactness' of the object, the source power scales with M^5 (not compact) or M^6 (compact).

The spectrum shape of vortex-shedding noise and trailing-edge noise is a function of both Strouhal number and Reynolds number; the spectrum shape of inflow-turbulence noise of Strouhal number only. On the basis of the M^6 scaling of the noise levels and a model for vortex-shedding noise, a general spectrum shape and a correlation formula for the aerodynamic broadband noise of the pantograph is formulated.

It is concluded that vortex shedding from various sharp and bluff parts of the pantograph is the most important noise producing mechanism. Inflow-turbulence noise as generated in the foot region, may also be important depending on the level and spectrum of the turbulence in the inflow (i.e. in the boundary layer along the train roof).

The results finally suggest that by optimising the shape of the pantograph top region, a reduction in the order to 10 dB can be obtained.

8. Acknowledgement

The research described is carried out under a contract awarded by the Dutch Ministry of Environmental Issues (Ministerie van VROM). This support is gratefully acknowledged.

The authors would further like to thank Mr. Blaskow of Adtranz GmbH for placing the pantograph available at the project and for his support during the test.

Furthermore, the contributions of Mr. Kooi, and of all other DNW employees committed to the preparation and performance of the test are gratefully acknowledged.

REFERENCES

1. Haaren, E. van, Parchen, R., *Aeroacoustic sources at high-speed trains* (in Dutch), NS Technical Research report no. NSTO/1/9610033/0001, 1996.
2. Dassen, A.G.M., Parchen, R., Bruggeman, J., Hagg, F., *Results of a Wind Tunnel Study on the Reduction of Airfoil Self Noise by the Application of Serrated Blade Trailing Edges*, EUWEC' 96 Conference Proceedings, Gothenburg, 20-24 May 1996.
3. Guidati, F., T. Dassen, R. Parchen, R. Bareiß, S. Wagner, *Simulation and Measurement of Inflow-Turbulence Noise on Airfoil Sections*, Proceedings of the 3rd AIAA/CEAS Aeroacoustics Conference, Atlanta, Georgia, May 1997.
4. Haykin, S., *Array signal processing*, Prentice Hall, Englewood Cliffs, N.J., 1985.
5. Johnson, D.H., Dudgeon, D.E., *Array signal processing - Concepts and Techniques*, Prentice Hall Signal Processing Series, Englewood Cliffs, N.J., 1993.
6. Hald, J., *STSF - a unique technique for scan-based Near-field Acoustic Holography without restrictions on coherence*, Brüel and Kjær Technical Review 1, 1989.
7. Leuridan, J., Roesems, D., Otte, D., *Use of principal component analysis for correlation analysis between vibration and acoustical signals*, Proceedings of the 16th International Symposium on Automotive Technology and Automation (ISATA Florence (Italy), 1987, pp. 487-504.
8. Cheng, D.K., *Optimization techniques for antenna arrays*, Proceedings of the IEEE, Vol. 59, No. 12, 1971, pp. 1664-1674.



9. Cox, H.; Zeskind, R.M.; Owen, M.M., Robust adaptive beamforming, *IEEE Proceedings on Acoustics, Speech and Signal Processing*, Vol. ASSP-35, No. 10, 1987, pp. 1365-1376.
10. Amiet, R.K., *Acoustic Radiation from an Airfoil in a Turbulent Stream*, *J. Sound Vib.*, Vol. 41, nr. 4, 1975.
11. Dowling, A.P., and Ffowcs Williams, J.E., *Sound and Sources of Sound*, Ellis Horwood Publishers, 1983.
12. Brooks, T.F., Pope, D.S., and Marcolini, M.A., *Airfoil Self Noise and Prediction*, NASA Reference Publication 1218, 1989.
13. Blake, W.K., *Mechanics of Flow-induced Sound and Vibration*, Academic Press inc., 1986, London.

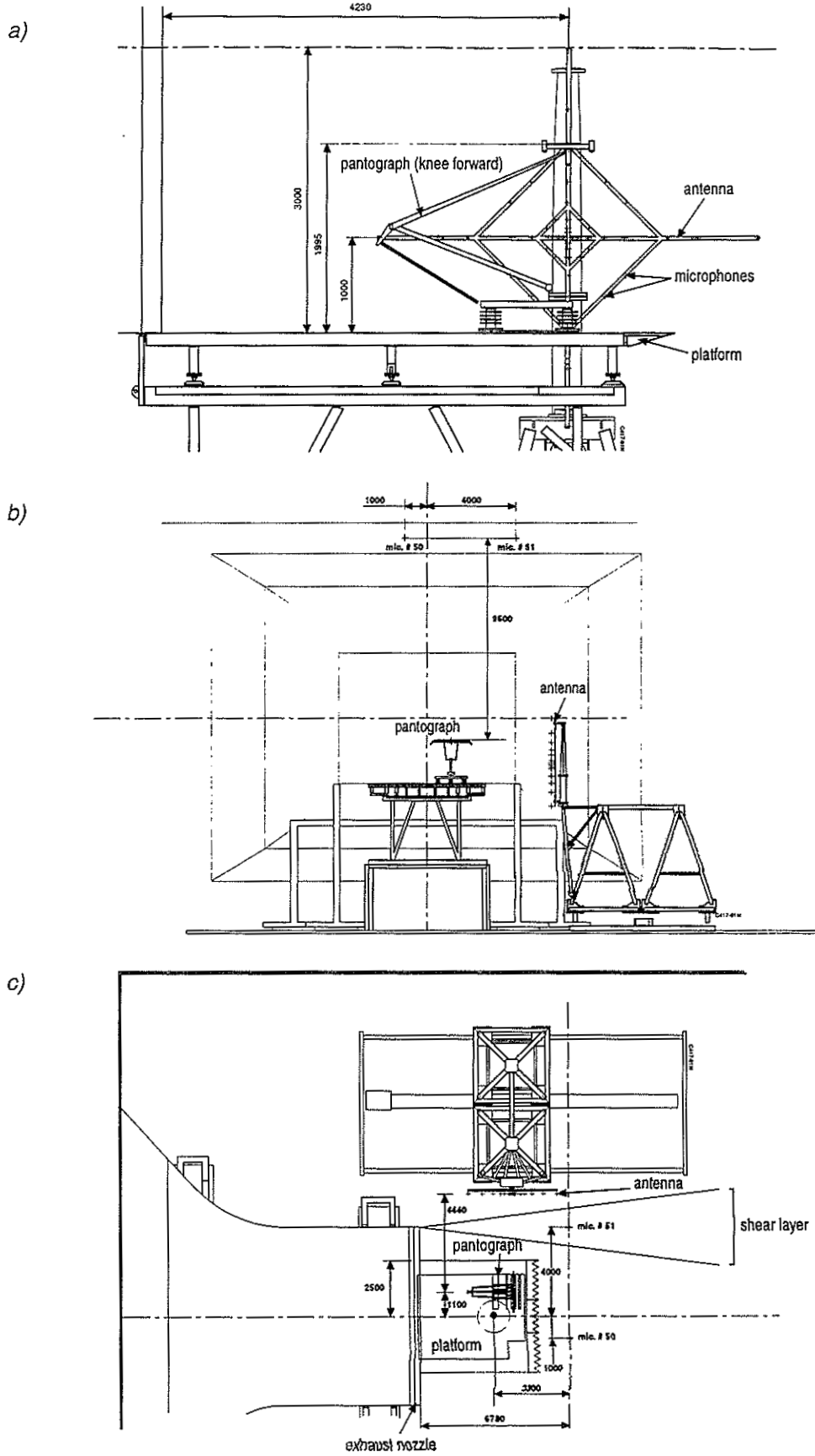


Fig. 2a-c Experimental set-up (side, front, and top view)

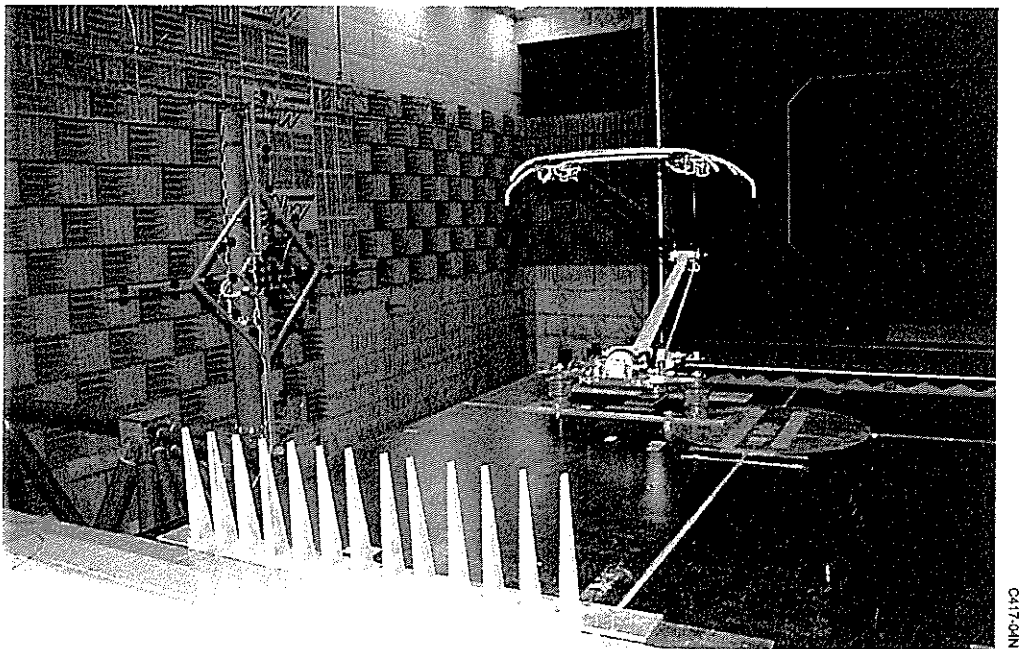
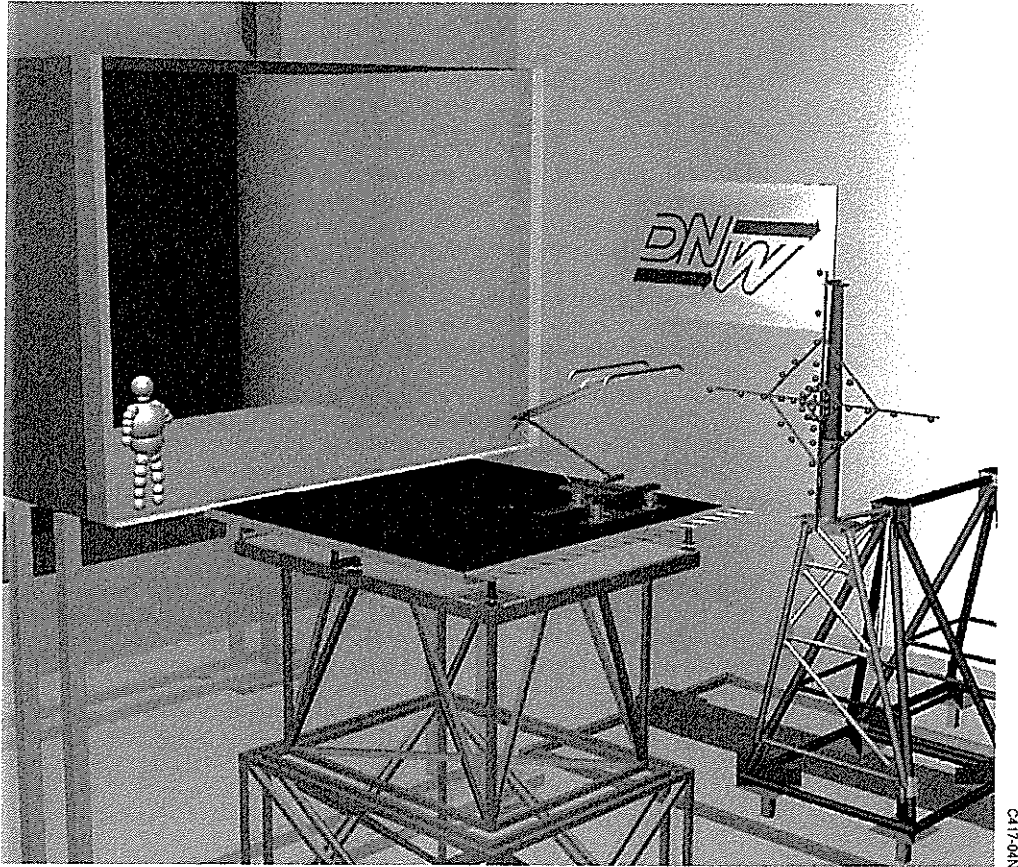


Fig. 3a-b Overview of experimental set-up (sketch, photographic picture)

| | |
|-----------------------|--------------|
| Run number | : 51 |
| Datapoint number | : 283 |
| Mach number [-] | : 0.23 |
| Temperature [K] | : 288.9 |
| Height pantograph [m] | : 1.95 |
| Configuration | : clean flow |

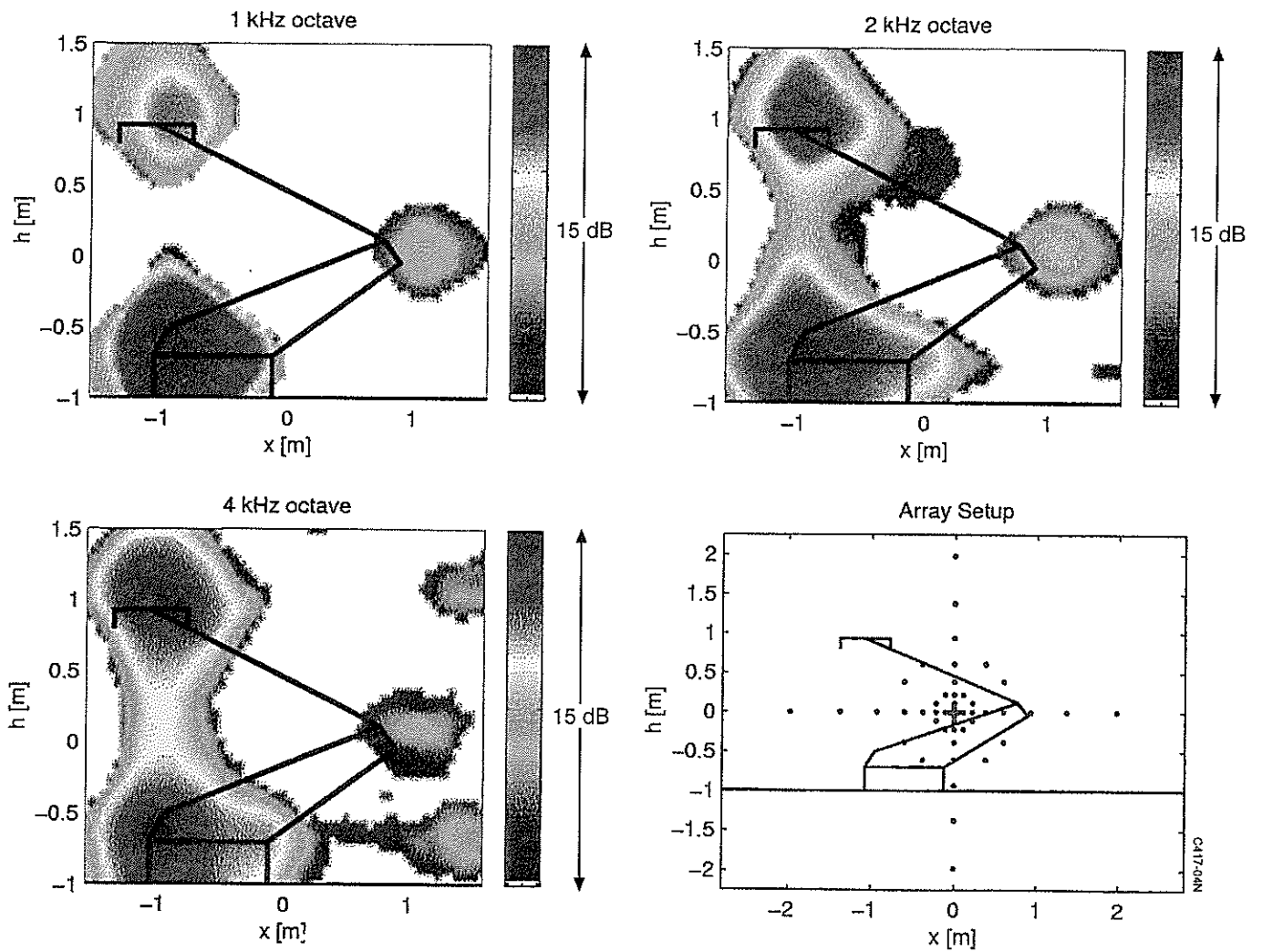


Fig. 4a Acoustic images

| | |
|-----------------------|--------------------|
| Run number | : 52 |
| Datapoint number | : 304 |
| Mach number [-] | : 0.23 |
| Temperature [K] | : 289.8 |
| Height pantograph [m] | : 1.95 |
| Configuration | : 180 deg. rotated |

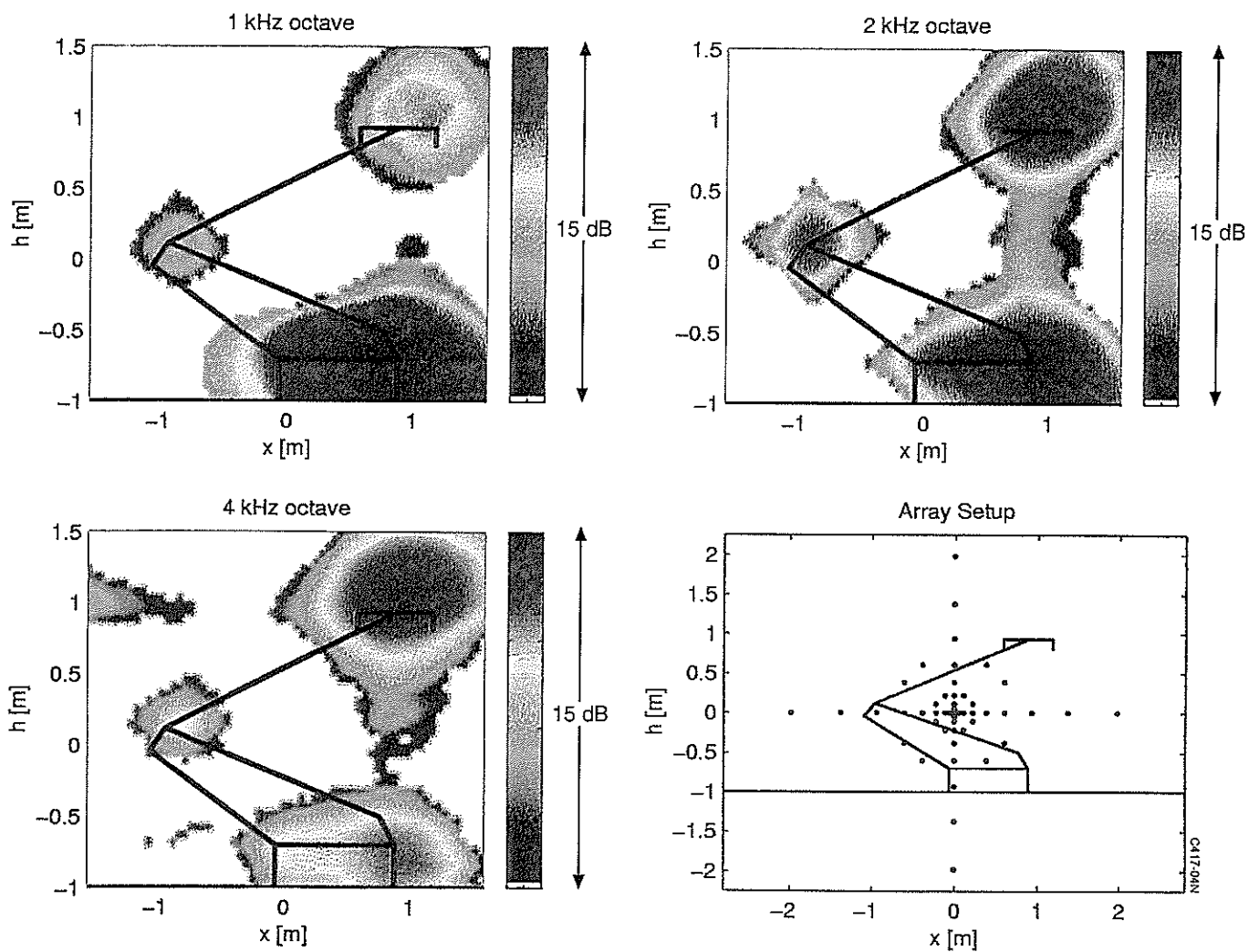


Fig. 4b Acoustic images

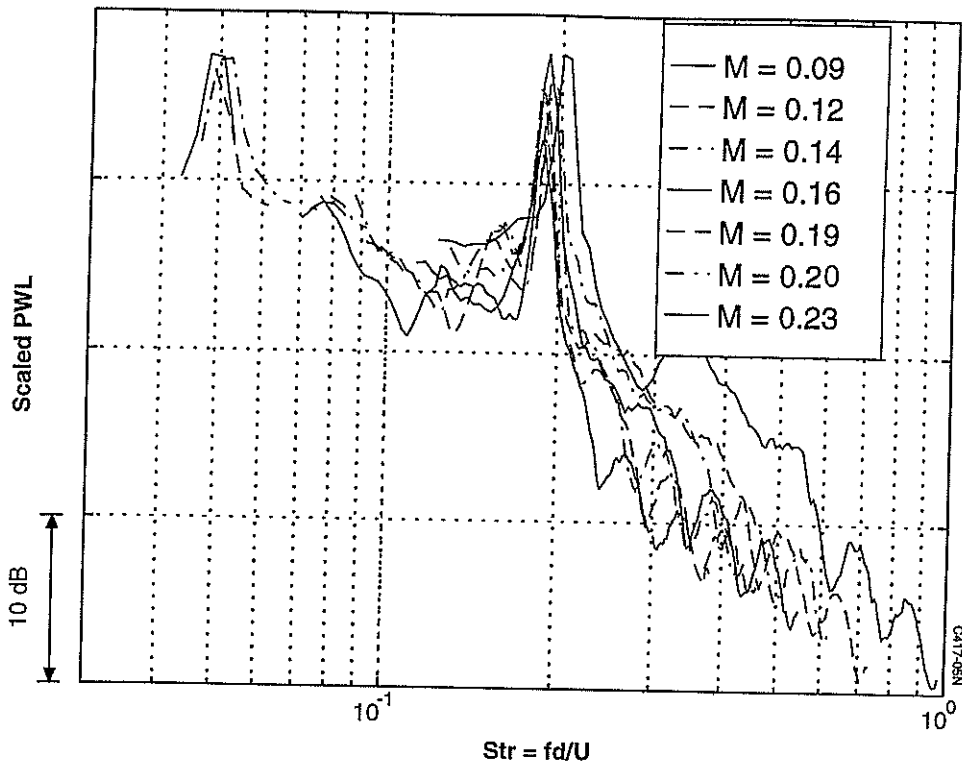


Fig. 5 Antenna measurements of the top region in the standard geometry

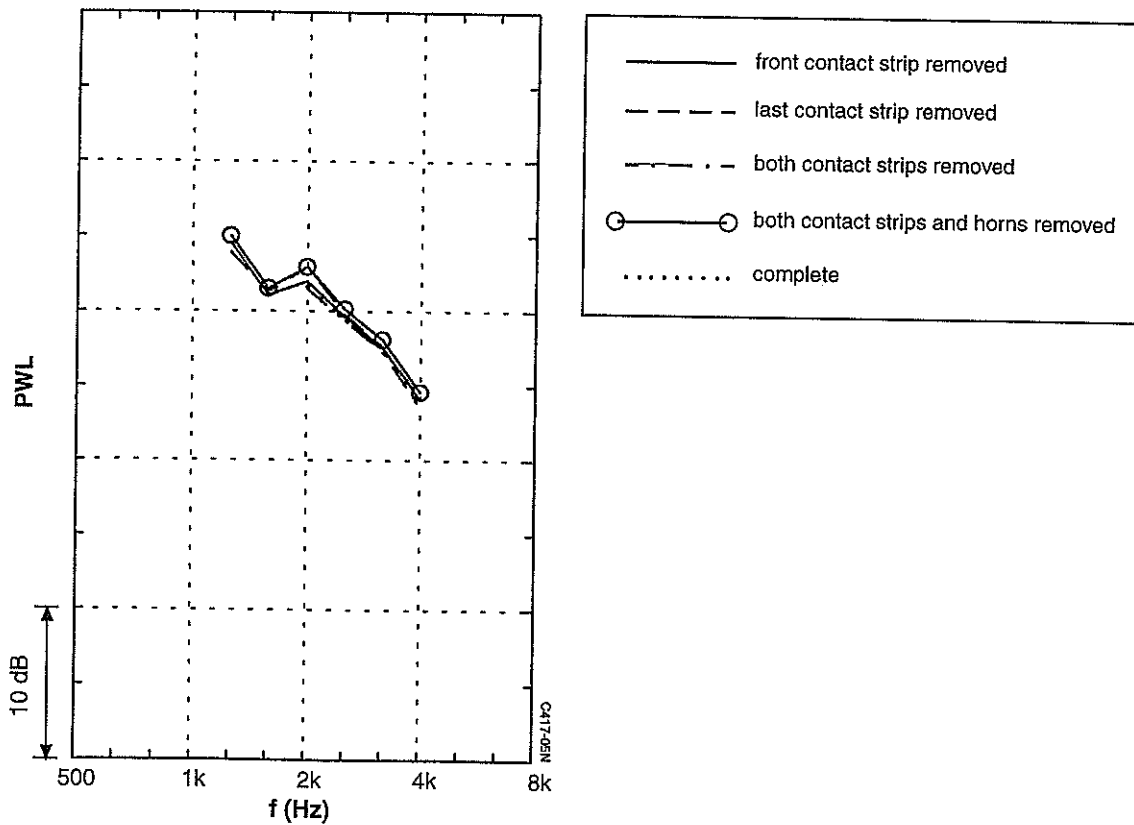


Fig. 6 Antenna measurements in 1/3 octave bands of the top region with parts of the pantograph removed

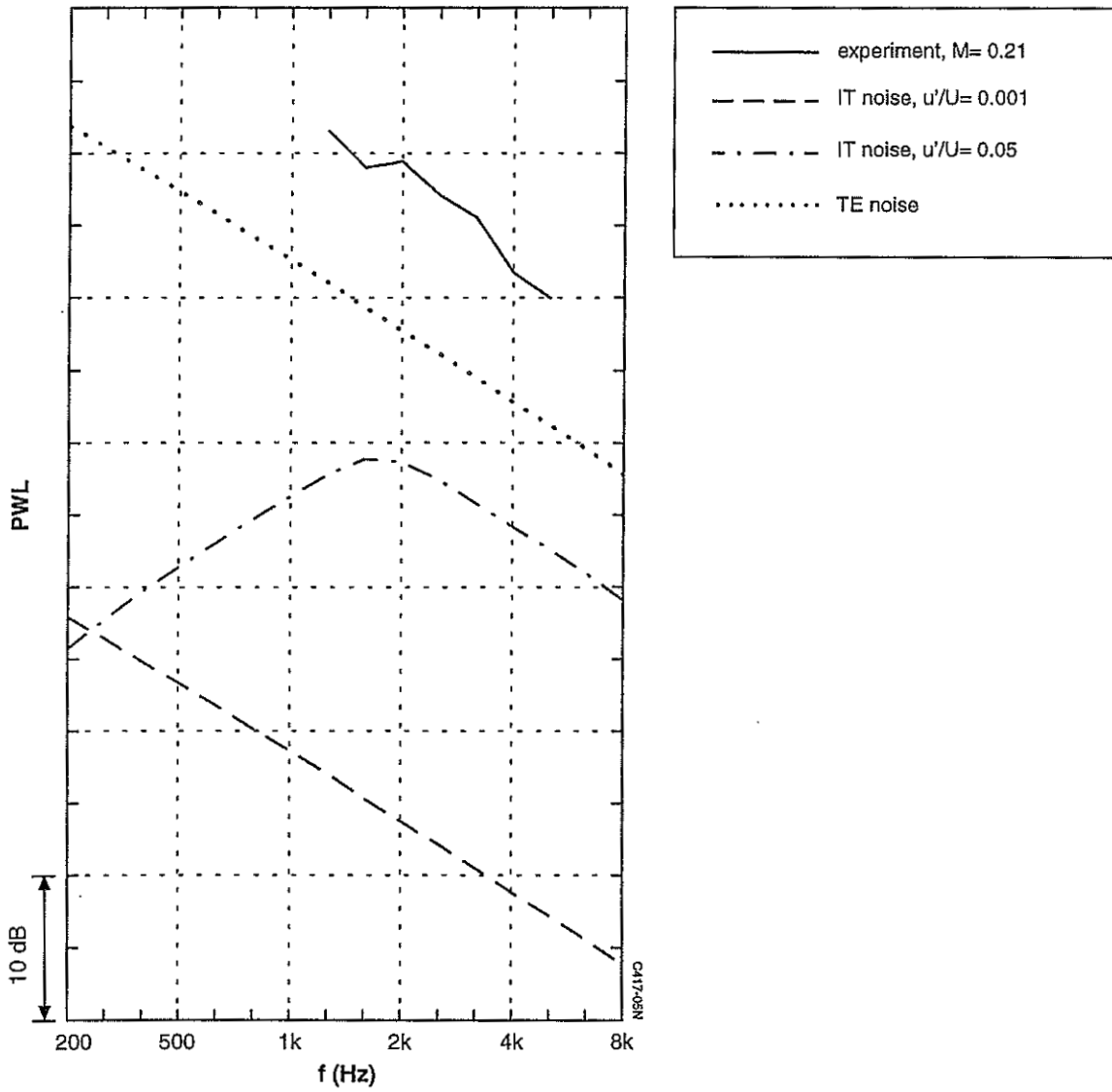


Fig. 7 Comparison of antenna measurements of the top region with predicted sound power level of an 1 m² flat plate for inflow-turbulence noise and boundary-layer trailing-edge noise

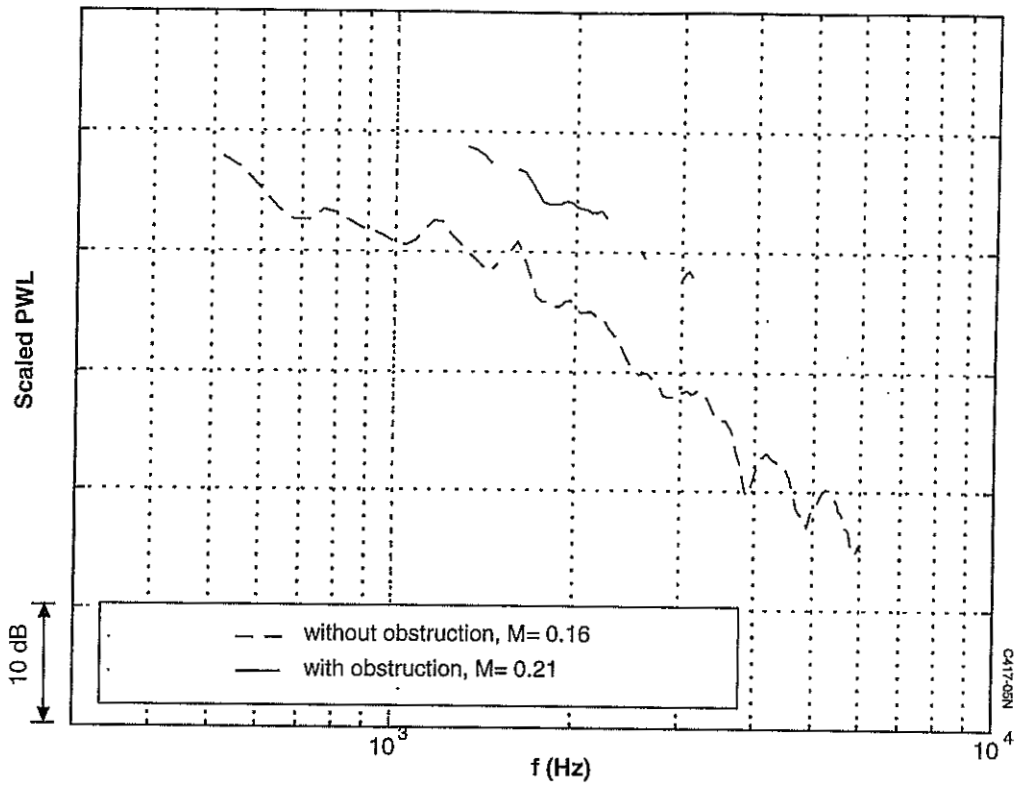


Fig. 8 Antenna measurements of the foot region with and without obstruction in the flow upstream of the pantograph

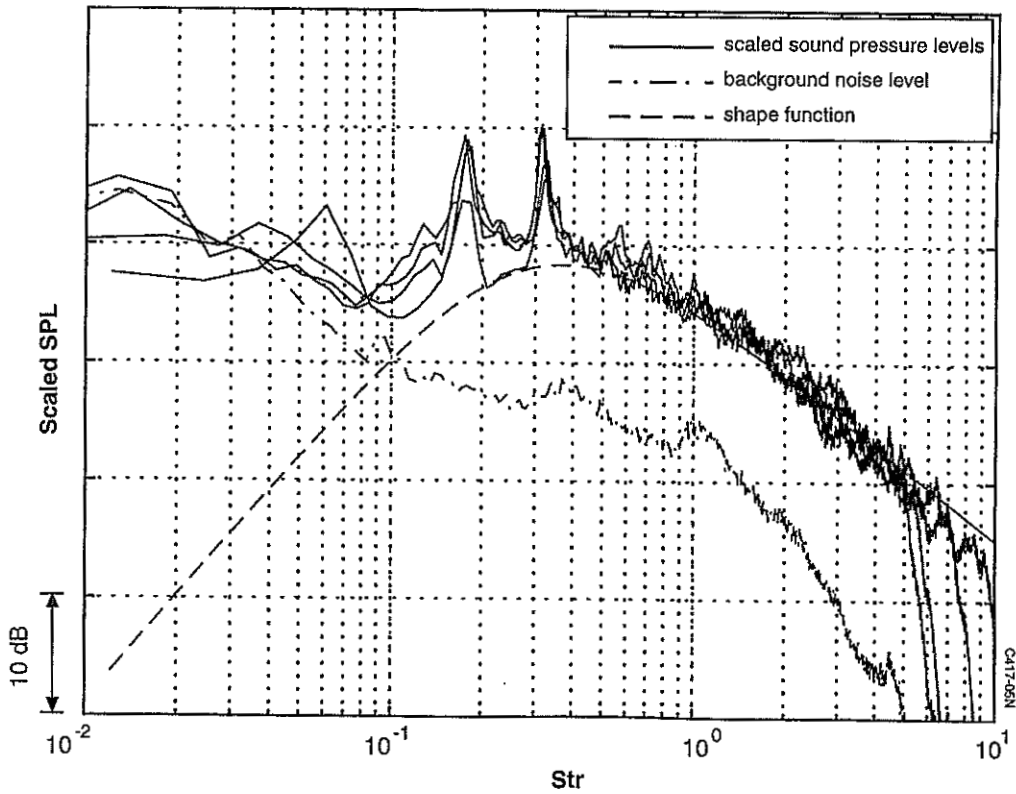


Fig. 9 Scaled sound pressure level measured by a single microphone. Also shown are the background noise level and a universal shape function for the broadband noise

